Ocean Modelling 167 (2021) 101875

Contents lists available at ScienceDirect

Ocean Modelling

journal homepage: www.elsevier.com/locate/ocemod

Generation mechanism of the counter-wind South China Sea Warm Current in winter

Zhitao Yu *, E. Joseph Metzger, Yalin Fan

Naval Research Laboratory, Stennis Space Center, MS, USA

ARTICLE INFO

Keywords:
South China Sea Warm Current
Wind relaxation
Ekman transport
HYCOM reanalysis
Topographic waves
Origin of South China Sea Warm Current

ABSTRACT

A 22-year (1994–2015) HYbrid Coordinate Ocean Model (HYCOM) global reanalysis is used to study the generation mechanism of the counter-wind characteristic of the South China Sea Warm Current (SCSWC) in winter seasons. Our analysis clearly demonstrates that the counter-wind SCSWC in winter is driven by wind relaxation. An Extended Empirical Orthogonal Function (EEOF) analysis of the hourly Sea Surface Height (SSH) and wind stresses reveals that the most dominant SSH mode is an Ekman mode. When the wind relaxes, the Ekman transport anomaly is offshore and generates a favorable cross-shore SSH slope for the northeastward surface currents over the continental shelf mainly by geostrophic balance. The alongshore pressure gradient force also increases when the wind relaxes, and dominates the weak wind stresses to push the alongshore water northeastwards. We also identify the region south of Taiwan Strait as the origin of the SCSWC, instead of the Hainan Island or Gulf of Tonkin, Vietnam due to the dominant Ekman dynamics.

1. Introduction

The semi-enclosed South China Sea (SCS) is the largest marginal sea in Southeast Asia (Fig. 1a). It connects with the East China Sea through Taiwan Strait, where the transport is generally northward (Chuang, 1985, 1986) even in the winter when northeasterly winds dominant the region. The SCS has a deep (>4000 m) central basin surrounded by a steep continental slope and links to the western Pacific through Luzon Strait, where the Kuroshio flows northward to the east of the strait and sometimes loops and sheds eddies through it, between Taiwan and Luzon. The deep central basin is bordered by a continental shelf, 150–250 km wide, shallower than 200 m along the coast of China (Fig. 1b).

In general, the dynamics of the upper layer circulation in the central SCS is fairly clear: the seasonally reversing East Asia monsoon wind plays a prominent role in forcing the seasonally varying circulation in the SCS (Wyrtki, 1961; Shaw and Chao, 1994). Northeasterly winds prevail over the region in winter while relatively weaker southwesterly winds dominate in summer. The wind driven basin-scale upper circulation is thus cyclonic in winter and anti-cyclonic in summer. However, the same is not true regarding the dynamics over the continental shelf in the northern SCS where a detailed topography is given in Fig. 1b. The northern SCS circulation is complex, including the shelf and slope circulation (Shu et al., 2018), summer Vietnam offshore currents (Shu et al., 2016), and the strong intra-seasonal variability of the cross-slope flow (Wang et al., 2020b). The subsurface speed maxima along the slope originates from Kuroshio intrusion through Luzon Strait (Wang et al., 2020a).

Historically, it was thought that the currents over the continental shelf in the northern SCS flow from northeast toward the southwest during the winter under the intense influence of the northeasterly monsoon (Wyrtki, 1961) until the South China Sea Warm Current (SCSWC) was observed in winter by Guan and Chen (1964) from the measured current data obtained by anchored stations and hydrographic characteristic analysis (Guan and Fang, 2006). Since then, the SCSWC has been confirmed by repeated observations (Guan, 1986; Guan and Fang, 2006) and was demonstrated as a narrow and strong northeastward current persisting all winter long (Su and Wang, 1987; Hu et al., 2000) and originating from Hainan Island (Li et al., 1992; Hu et al., 2000; Guan and Fang, 2006; Yang et al., 2008). In winter, it is sandwiched between the southwestward Guangdong Coastal Currents and the southward currents along the shelf break that are related to the wind-driven cyclonic gyre in the SCS (Qiu et al., 1985; Guan, 1993). The trademark of the SCSWC is its counter-wind characteristic in winter. Over a half century after the SCSWC was discovered, scientists have proposed different generation mechanisms trying to explain its counter-wind behavior in winter.

The main proposed generation mechanism is Kuroshio intrusion into the SCS via Luzon Strait. Su and Wang (1987) employed a barotropic model with zero wind stress and suggested that Kuroshio intrusion plays an important role on the SCSWC formation. The importance of the Kuroshio is evident in Zhong (1990) who indicated that the formation

* Correspondence to: Ocean Sciences Division, Naval Research Laboratory, Stennis Space Center, MS 39529, USA.
E-mail address: zhitao.yu@nrlssc.navy.mil (Z. Yu).

https://doi.org/10.1016/j.ocemod.2021.101875
Received 5 February 2021; Received in revised form 8 July 2021; Accepted 30 July 2021
Available online 3 September 2021
1463-5003/Published by Elsevier Ltd.

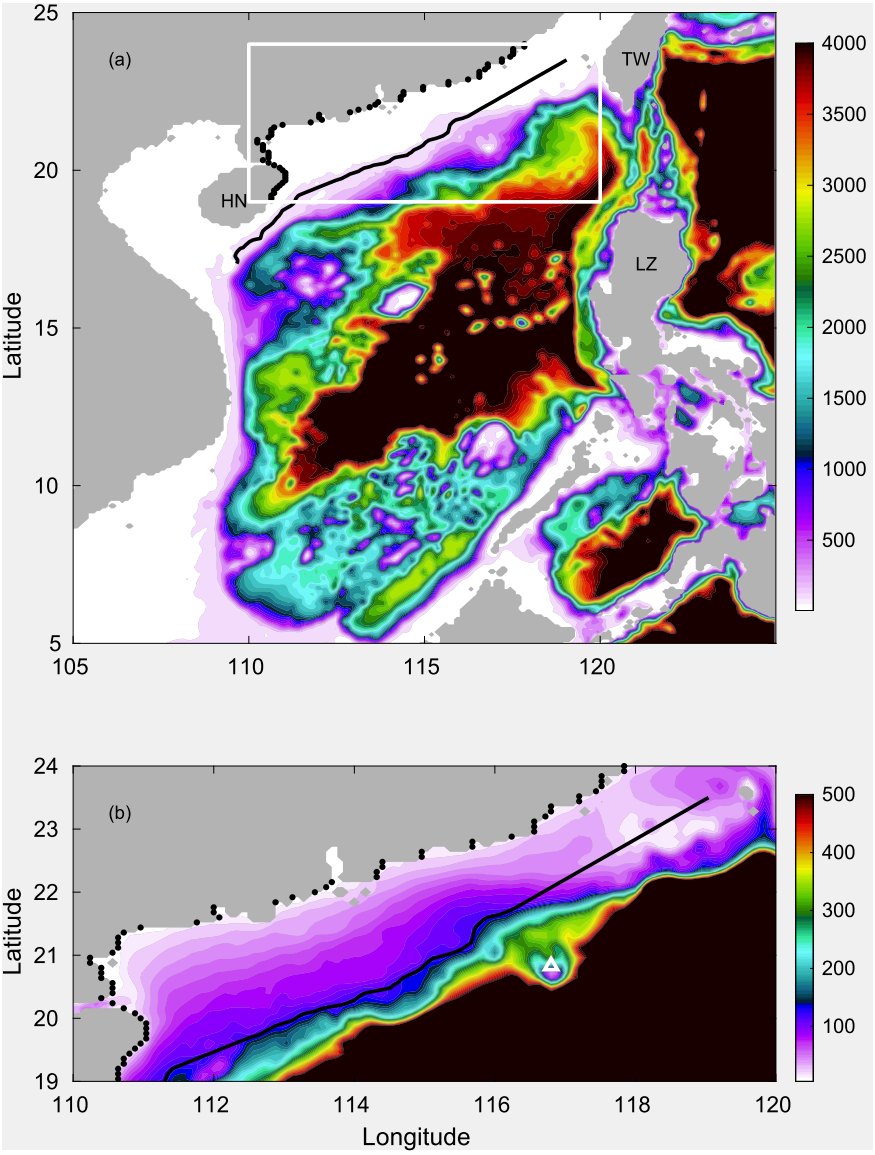

Fig. 1. HYCOM bathymetry (meters) for the South China Sea (a) and the region for this study (b). Gray represents model land points. Taiwan (TW), Luzon (LZ), and Hainan Island (HN) are labeled. The white box in (a) defines the region of interest of this study. The white triangle in (b) represents Dongsha Island. The land–ocean boundary is defined by the 10 cm isobaths but all depths less than 5 m are set to 5 m. The black line defines the path of the South China Sea Warm Currents used to generate Fig. 8b. The black dots denote the coastline grid points used for sea surface high anomaly Hovmöller diagram in Fig. 8a.

of the SCSWC is dynamically related with the South China Sea Branch current of the Kuroshio. Ye (1994) demonstrated that the temperature increase from shelf to slope due to the warm winter Kuroshio intrusion onto the slope could generate northeastward geostrophic flow. Xue et al. (2004) also linked the formation of the SCSWC to Kuroshio intrusion. However, the numerical experiments conducted by Li et al. (1993) demonstrated that Kuroshio intrusion is not a requirement for the formation of SCSWC but may only strengthen the SCSWC. Their results showed that the SCSWC still exists but appears to be weaker if Luzon Strait is closed. Similar conclusions were made by Yang et al. (2008).

Another proposed generation mechanism is related to the alongshore Sea Surface Height (SSH) slope. Zeng et al. (1989) hypothesized that the alongshore pressure gradient induced by the water piled up to the east of Hainan Island forces the northeastward flow. Numerical results from barotropic simulations of the Pacific Ocean by Li et al. (1992) indicated that the combined effect of cross-shore and alongshore sea surface slope is probably one of the major forces driving the SCSWC. Chao et al. (1995) were the first one to suggest the wind relaxation as a possible generation mechanism when the alongshore SSH slope exists. Their numerical simulations clearly demonstrated the formation of the SCSWC when wind relaxes in winter. They conclude that the monsoon-driven southwestward coastal current piles up water downwind near Hainan Island to generate the alongshore SSH slope and the alongshore northeastward pressure gradient force drives the SCSWC after wind relaxes. Yang (2006) found that the northeastward currents over the shelf appears only when the northeast monsoon is weak based on mooring observations from 5 November 2001 and 21 March 2002 (T1 in Fig. 1b of Yang (2006)). Chiang et al. (2008) examined the idea using a fine resolution (1/16°) Princeton Ocean Model (POM) and confirmed that the wind relaxation is the dominant winter SCSWC generation mechanism since the northeastward pressure gradient force takes place only when the northeasterly monsoon relaxes. However, our analysis has raised some questions regarding their results. As shown in Section 3, while mean SSH clearly shows a northeastward pressure gradient force, there are no mean northeastward currents associated with it. On the other hand, Hsueh and Zhong (2004) explained the formation of the SCSWC applying the coastal arresting wave theory

(Csanady, 1978) but attributed the along shelf pressure gradient to the collision of the Kuroshio intrusion currents with the continental slope.

Besides the above research, the following provide a different point of view on the formation of the SCSWC. The importance of Taiwan Strait was illustrated through numerical simulations by Yang et al. (2008) who demonstrated that the SCSWC vanishes when the Taiwan Strait is closed. They suggested that the SCSWC is a source and sink-driven flow induced by the year-round northward flow through the Taiwan Strait. The wind stress applied to their numerical simulation is a 4-year average derived from observations by NASA satellite scatterometers. Wang et al. (2010) performed numerical experiments using POM and revealed that it is the Joint Effect of Baroclinicity and Relief (Sarkisyan and Ivanov, 1971) that drives the SCSWC against the wind in winter. This effect forces the slope currents to flow across the isobaths and veer to the right hand to feed the SCSWC. The onshore pressure gradient force in the outer continental shelf that is favorable for the northeastern SCSWC comes from Kuroshio intrusion via the Luzon Strait.

From the previous research, it is fair to say that there still is no agreed upon consensus within the scientific community for the dynamics that controls the SCSWC. Recent observations and numerical simulations also question the persistency of the SCSWC in the winter, which further complicates the situation. Fang et al. (2015) did not observe the presence of SCSWC over the continental shelf in the northern SCS in 2006 and 2007. And the hypothesis of wind relaxation (Chao et al., 1995; Chiang et al., 2008) implies that the SCSWC is not persistent but rather intermittent. But all of these previous numerical results agree on one or both of the two physical conditions: an onshore and/or a northeastward alongshore pressure gradient force exists over the continental shelf. The onshore pressure gradient force indicates that the SCSWC is mainly in geostrophic balance in the cross-shore direction, while the northeastward alongshore pressure gradient force implies that the SCSWC is not in pure geostrophic balance but ageostrophic in alongshore direction, which allows alongshore wind stress and/or bottom friction to be important dynamically as well. Thus, there are two sets of equations, geostrophic in cross-shore and ageostrophic in alongshore, to govern the SCSWC. The generation mechanism has to satisfy both. And thus, what mechanism generates both cross-shore and alongshore pressure gradient that favor the formation of SCSWC?

In this study, we further examine the generation mechanisms of the counter-wind characteristic of the SCSWC in winter seasons. Results from a 22-year global HYbrid Coordinate Ocean Model (HYCOM) data-assimilative reanalysis are carefully analyzed and demonstrated that wind relaxation is the dynamical reason driving the counter-wind characteristic of the SCSWC in winter. There are two pathways, direct and indirect, via which the SCSWC is affected by the wind relaxation. The direct pathway is that wind stress represents a weaker force in the alongshore direction, while the indirect pathway refers to the offshore Ekman transport due to the wind relaxation. Previous studies on wind relaxation attribute the alongshore pressure gradient to the blockage effect of Hainan Island (Chao et al., 1995) or the Gulf of Tonkin (Chiang et al., 2008) but do not explain what sets up the onshore pressure gradient force. This research differs and improves on previous studies in that (1) we found that wind relaxation sets up the favorable onshore pressure gradient force over the continental shelf via Ekman transport, contrary to Chiang et al. (2008) who stated that Ekman transport is not important in maintaining the SCSWC, (2) wind relaxation is the reason why there is a need to have alongshore counter-wind currents in winter — so that the bottom friction, opposite to the current direction, follows the northeasterly monsoon wind to balance the northeastward alongshore pressure gradient force, (3) unlike previous numerical studies, the HYCOM reanalysis was forced by hourly wind stress and fluxes and thus is able to fully resolve physical processes with a time period less than one day, and (4) our findings indicate the SCSWC originates in the area south of Taiwan Strait, contrary to the commonly accepted origination near Hainan Island or Gulf of Tonkin, Vietnam. The same reanalysis was used to study the surface wind work input into the global ocean. The high temporal resolution of the wind stress fills the missing wind work spectrum due to the low temporal forcing resolution (i.e. daily) and increases the wind work over ageostrophic currents significantly (Yu et al., 2018). To our knowledge, this is the first time that a reanalysis with such a high temporal resolution is used to study the SCSWC dynamics. More details of the reanalysis are provided in Section 2.

This paper is organized as follows: Section 2 introduces the numerical model configuration and data assimilation method for the reanalysis. Section 3 describes the monthly mean characteristics of the SSH, wind stresses, and the surface currents. Basic statistics of the SCSWC are summarized in Section 4. An Extended Empirical Orthogonal Function (EEOF) analysis of the hourly SSH and wind stress anomalies are presented in Section 5. The alongshore forcing comparison is performed in Section 6. Some of the observed features of the SCSWC are explained and the origin of the SCSWC is defined in Section 7, which is followed by conclusions in Section 8.

2. Numerical model and simulations

A 22-year global HYCOM reanalysis from 1994 to 2015 is used for this study. HYCOM is the ocean model component for the present operational US Navy Global Ocean Forecast System (Metzger et al., 2014). A detailed description of HYCOM physics is provided by Bleck (2002). A brief description of the model setup is presented below with emphasis on the numerical aspects that are most relevant to this study. There are no tides or surface waves in this reanalysis.

2.1. Model grids and output

The HYCOM horizontal resolution for the reanalysis is 0.08° (1/12.5°) that is ~9 km at the equator and ~6.5 km at mid-latitudes. The grid is uniform cylindrical from 78.64°S-66°S, Mercator between 66°S-47°N and includes a bipolar patch north of 47°N providing ~3.5 km grid spacing at the North Pole. The bathymetry is derived from 30 arc-second General Bathymetric Chart of the Oceans (GEBCO, https://www.gebeo.net). Three coordinates coexist in HYCOM vertically: z-coordinates in unstratified water, sigma-coordinates in shallow depths, and isopycnal coordinates in the stratified ocean. Hence, HYCOM maintains the significant advantages of an isopycnal model in the stratified ocean, but allows coordinate surfaces to locally deviate from isopycnals to provide more vertical resolution near the surface and in shallow coastal regions in order to better represent the upper ocean physics (Chassignet et al., 2003). With this unique feature, HYCOM serves as a good tool for simulating circulations in the SCS, which has complex topography that covers the continental shelf and deep basin. There are 41 hybrid coordinate layers vertically with potential density referenced to 2000 m. The top 14 layers are always sigma-z so that water shallower than 84 m is always in fixed coordinates. For this study, we mainly analyze wind stresses and SSH output. Hourly instantaneous wind stress and SSH fields are interpolated to a uniform 0.08° resolution. Three dimensional velocity fields are saved 3-hourly.

2.2. Data assimilation

The data assimilation technique employed for the reanalysis is a 3D variational scheme used within the Navy Coupled Ocean Data Assimilation (NCODA) (Cummings, 2005; Cummings and Smedstad, 2013) that takes the 24-hour model forecast as a first guess. Available remotely sensed sea surface temperature (SST), SSH, sea ice concentration, and in-situ observations of temperature and salinity from profiles, ships, and moored and drifting buoys are all assimilated into HYCOM. NCODA also generates synthetic temperature and salinity profiles for assimilation that are formed from the two-dimensional SSH and SST using a 3D synthetic profile method, the Improved Synthetic Ocean Profile

(ISOP, (Helber et al., 2013)). ISOP provides an accurate representation of the ocean's temperature and salinity vertical gradient as defined by historical in-situ observations. The reanalysis provides realistic SSH fields as verified by Cummings and Smedstad (2013) who showed the assimilated SSH field in the Kuroshio region is in good agreement with independent infrared frontal analyses.

2.3. Initialization and surface forcing

The 22-year reanalysis is not continuous but separated into streams to speed the time to solution when it was integrated. Most of the streams are 2.5 years long. For each stream, the initialization state comes from a previous 20-year HYCOM-based reanalysis (Yu et al., 2015) on 1 December of the previous year except the very first stream started on 1 June 1993.

The reanalysis uses atmospheric forcing from the 0.3125° hourly NCEP Climate Forecast System Reanalysis (CFSR) (Saha and Coauthors, 2010). The wind stress formulation in the model includes the ocean surface currents (Yu et al., 2017). The NCEP CFSR 10-m wind velocities are read by HYCOM and the wind stress is calculated at every time step taking into account the ocean surface currents as shown below

$$\boldsymbol{\tau} = \rho_{air} C_d \left|\boldsymbol{V_{10}} - \boldsymbol{V_o}\right| (\boldsymbol{V_{10}} - \boldsymbol{V_o}), \quad (1)$$

where ρ_{air} is the air density at sea level, C_d is the drag coefficient, and $\boldsymbol{V_{10}}$ is the 10-m wind velocity, and $\boldsymbol{V_o}$ is the velocity of ocean surface currents at 1 m depth. This wind stress formulation is more accurate and generates larger wind stresses when the SCSWC flows counter to the prevailing winds compared to calculating wind stress with 10-m winds only.

The previous 20-year HYCOM-based reanalysis used to initialize this reanalysis does not include the ocean surface currents in the wind stress formulation. When the new wind stress formulation (including ocean surface current) is applied during the reanalysis, the mesoscale eddy field adjusts to the satellite altimeter data within the first month (Yu et al., 2015) but the basin wide kinetic energy takes another 6 months to reach an "equilibrium" (Yu et al., 2018). Thus, while the ~2.5-year streams start on December 1 of the previous year and end after 31 months of integration, i.e. the end of June, only the last two years of output (e.g. July 2001 to June 2003) from each ~2.5-year stream are used in the analysis here.

2.4. Region of interest

We focus on the northern SCS for this study and the domain chosen is from 110° – 120°E, 19° – 24°N (white box in Fig. 1a, Fig. 1b). Its southwestern boundary covers part of the Hainan Island and the northern boundary is to the south of Taiwan Strait. Its eastern boundary is to the west of Luzon Strait. This region is big enough to cover all the SCSWC over the northern SCS continental shelf and small enough to eliminate most of the impact of central basin variations for the EEOF analysis.

3. Monthly mean model results

The monthly mean SSH and alongshore wind stresses are removed from the EEOF analysis. These mean fields are important to interpret the EEOF results. For instance, the EEOF shows that SSH decreases over the continental shelf when the wind relaxes (Section 5.1) and the associated geostrophic flow anomaly is northeastward. But this does not mean there are counter-wind currents. The counter-wind SCSWC exists only when the SSH decrease overturns the mean SSH cross-shore slope based on geostrophic balance. Thus, the monthly mean SSH, alongshore wind stresses, their associated standard deviation (STD), and mean surface currents of December 1994 are shown as examples in this section. We choose to show results in December 1994 because it contains one of the longest SCSWC occurrence during the 22-year reanalysis. More detailed analysis during this period is given in Section 4. The fundamental pattern over the continental shelf described below applies to all the winter seasons (December, January, February) during the 22-year reanalysis period.

3.1. Sea surface height

The mean December 1994 SCS SSH (Fig. 2a) clearly shows the two important features of the northern SCS general circulation: the cyclonic circulation in the deep basin and the Kuroshio intrusion through Luzon Strait. The Kuroshio, identified by the high SSH, intrudes more water into the SCS through Luzon Strait in December (6.4 Sv, 22-year average) than summer (0.5 Sv). This agrees well with observations (Tian et al., 2006). The cyclonic circulation in the deep basin, represented by the low SSH in Fig. 2a, across the basin from 9° to 21°N, agrees with previous research (Wyrtki, 1961).

Along the continental shelf, mean SSH in December 1994 is higher nearshore and decreases offshore gradually, and lower near Taiwan Strait and increases southwestwards over the shelf (Fig. 2b). The low SSH in the deep central basin is consistent with the basin wide cyclonic circulation in the winter. The higher SSH to the east of 118°E between 20.5° and 22.5°N is associated with Kuroshio intrusion through Luzon Strait. The mean SSH pattern indicates an offshore pressure gradient force, which agrees well with TOPEX/Poseidon altimetry data (Shaw et al., 1999; Ho et al., 2000; Chu et al., 2003; Fang et al., 2006) and does not suggest the existence of northeastward currents via geostrophic balance. Another important feature of the mean SSH over the shelf is that there exists a clear alongshore pressure gradient, higher SSH in the vicinity to the northeast of the Hainan Island and lower at Taiwan Strait. According to previous research (Zeng et al., 1989; Chiang et al., 2008), the alongshore pressure gradient suggests surface water flows northeastward, i.e. down gradient.

The STD of SSH indicates that most of the SSH variations occur over the continental shelf, higher along the coast and decreasing offshore (Fig. 2c). The strongest variation of SSH occurs near Taiwan Strait. The SSH variation in the central basin is much smaller than that over the continental shelf. The small SSH STD of the South China Sea Branch current of the Kuroshio in a band roughly in line with the 200 m isobath indicates that SSH variations associated with the Kuroshio do not change much and thus cannot be the primary cause of the SCSWC via geostrophic balance, agreeing with Li et al. (1993) and Yang et al. (2008).

3.2. Wind stresses

For wind stresses, we choose coordinates so that the y-axis (alongshore) coincides with the coast, positive towards northeast and the positive x-axis points offshore. The coastline is not straight and we estimate that the y-axis is 38° to the north of east. It is very clear that the mean alongshore wind stresses are southwestward, negative, in December 1994 (Fig. 3a). There exists a strong mean alongshore wind stress band, strongest at Taiwan Strait and extending southwestward. The wind stresses are much weaker both to the southeast and northwest of this strong band (Fig. 3a). This pattern agrees well with climatology (Fang et al., 2006). The STD of wind stresses shows a similar spatial pattern as the mean wind stresses, with a strong variational band from Taiwan Strait and extending southwestward with the maximum STD near Taiwan Strait. Surface wind stresses to the southeast and northwest of this band do not change much. This STD pattern suggests that there are larger variations associated with stronger winds than the weak winds (Fig. 3b).

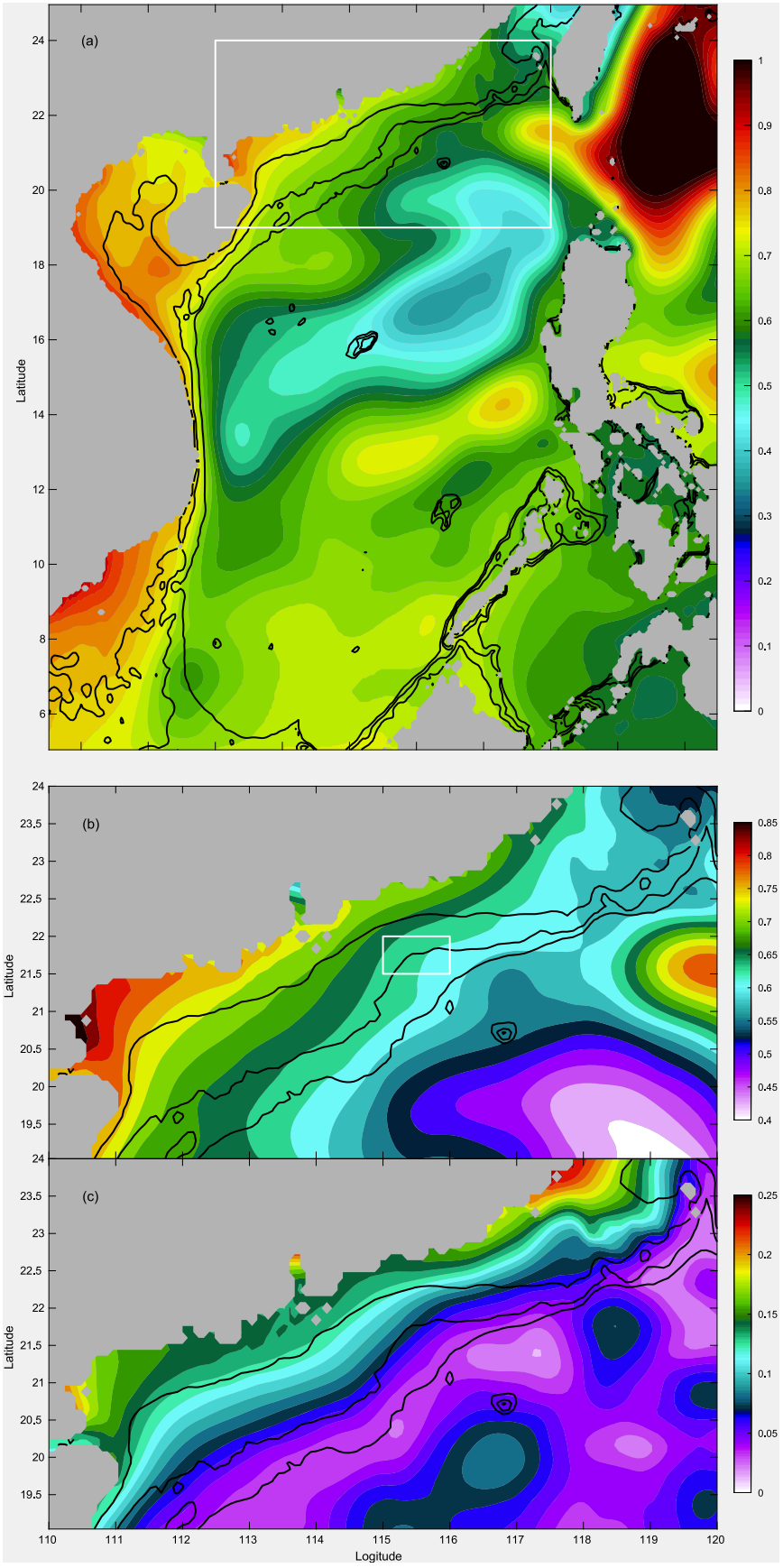

Fig. 2. South China Sea monthly mean Sea Surface Height (a, meters) in December, 1994 from the HYCOM reanalysis. The white box in (a) defines the region of interest of this study. Monthly mean (b, meters) and standard deviation (c, meters) of Sea Surface Height in December, 1994 in the white box in (a). The three black solid lines indicate the 50, 100, and 200 m isobaths, respectively. The white box in (b) defines the region of the South China Sea Warm Current detection.

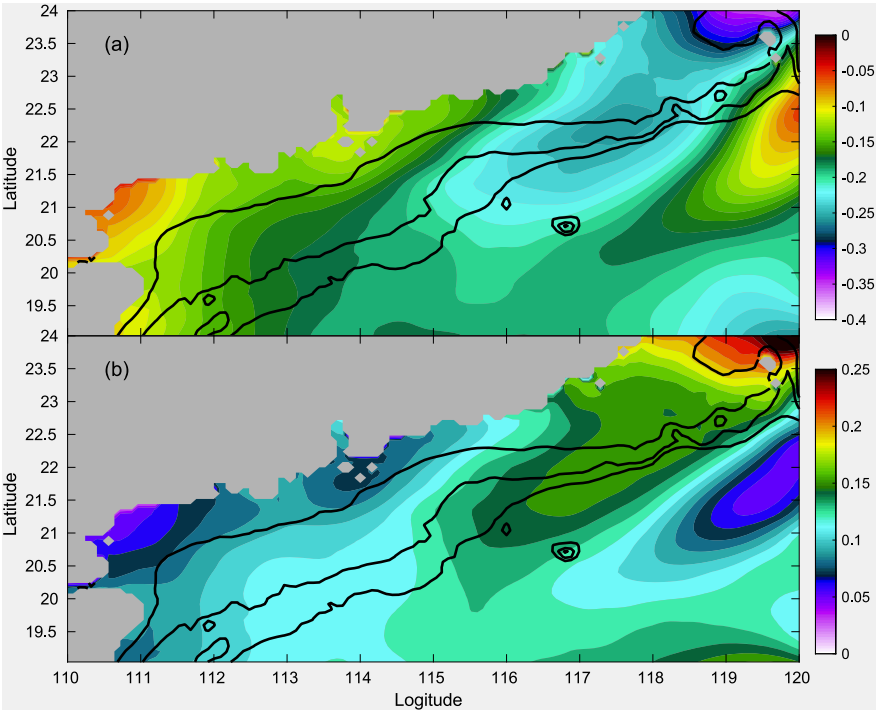

Fig. 3. Monthly mean (a, N/m^2) and standard deviation (b, N/m^2) of alongshore wind stress in December, 1994 from the HYCOM reanalysis. The three black solid lines indicate the 50, 100, and 200 m isobaths, respectively.

3.3. Near-surface currents

It was shown that sometimes the SCSWC flows beneath the ocean surface while the currents at the surface follow the wind direction (Guan and Fang, 2006). Thus, we show the currents, averaged over the top 50 m in the region of interest to represent the surface currents as suggested by Chiang et al. (2008). The monthly mean near-surface currents show no signature of the SCSWC over the continental shelf in December 1994 (Fig. 4), as suggested by the mean SSH in the same month via geostrophic balance over the continental shelf (Fig. 2b). Instead, the monthly mean near-surface currents mainly flow southwestward over the continental shelf, following the wind. Over the 22 year reanalysis time period, none of the winter monthly mean near-surface currents indicates the existence of SCSWC, agreeing with previous studies that suggested the SCSWC does not persist throughout the winter seasons (Chao et al., 1995; Yang, 2006; Chiang et al., 2008). We will provide an explanation for this in Section 7.

4. Statistics of the SCSWC

In this section, we summarize some basic statistics of the SCSWC from the reanalysis. These statistics include the occurrence rate, duration, length, magnitude, and the location of the SCSWC. These statistics are calculated from the daily-average HYCOM output.

Based on previous observations (Zhong, 1990), we decide to detect the SCSWC using the upper 50 m-average alongshore velocity in the rectangular area from 115° to 116°E and 21.5° to 22°N. This area is between the 50 and 200 m isobaths and on top of 100 m isobath (white box, Fig. 2b). We focus on the area less than 200 m because it is hard to find continuous counter wind currents between 200 and 300 m isobaths. This is in good agreement with the small SSH STD roughly along the 200 m isobath (Fig. 2c, Section 3.1). If the area averaged alongshore velocity in this area is positive, the SCSWC exists on that day. An event of the SCSWC is defined as the currents occurring on consecutive days or one day only, a one-day event.

There are 546 days of the SCSWC occurrence in the 21 winters. On average, there are 26 days of the SCSWC occurrence per winter and 9.5 SCSWC events with an average event duration of 2.7 days.

We also examine the daily averaged SSH and upper ocean currents when the SCSWC occurs to determine its location and magnitude. Somewhat surprisingly, the SCSWC generally does not exist near Hainan Island, but instead exists hundreds of kilometers to the northeast. Does this suggest that the SCSWC originates on the shelf away from Hainan Island? The SCSWC only spans the whole continental shelf from Taiwan to Hainan Island (more than 1100 km) when an event lasts three days or longer. During such events it can reach the Gulf of Tonkin, Vietnam at 18°N. For one-day events, the SCSWC usually exists northward of 21°N towards Taiwan Strait, which is 400 km long.

The positive alongshore velocity of the SCSWC can reach to 150 m depth. The barotropic alongshore velocity is as large as 0.28 m/s along the 100 m isobath and reached 0.10 m/s along the 200 m isobath in the December 1994 event shown below.

5. EEOF analysis of SSH and wind stress anomaly

A fundamental response over the continental shelves to the wind forcing expected from dynamics is the generation and propagation of the coastal topographic waves. Jacobs et al. (1998) demonstrated that wind bursts and relaxation excite coastal topographic waves in the East China Sea (their Figure 3). These waves then propagate southwards along the continental shelf and pass through Taiwan Strait (Ko et al., 2003). Chao et al. (1995) observed that the emergence of the northeastward SCSWC begins from the northeastern shelf (115°E, 21°N) after wind relaxation and expands southwestward. They attributed this to the propagation of topographic waves. From the daily-average SSH animation generated from the reanalysis, we often see a wave-like feature with lower SSH than that near Hainan Island propagate southwestwards from the southern end of Taiwan Strait along the continental shelf as a precursor to the SCSWC in winter. Is this wave-like feature a topographic wave?

In this section, we perform an EEOF analysis on the hourly SSH and wind stress anomalies. We choose EEOF over EOF because it

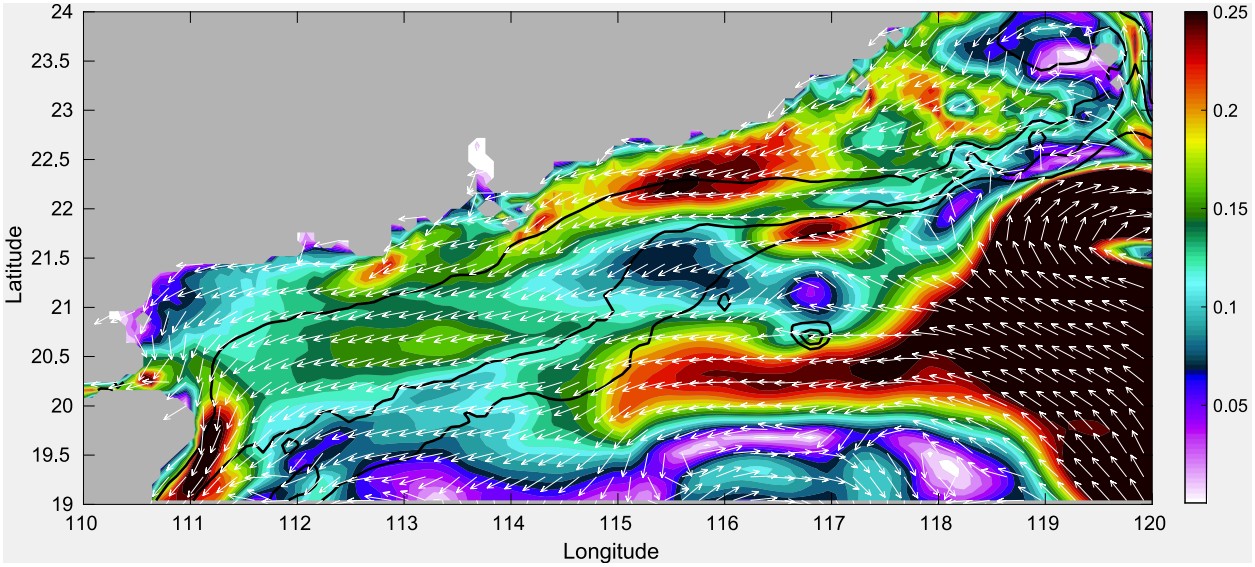

Fig. 4. Monthly mean near-surface currents (m/s) averaged over the top 50 m in December 1994 from the HYCOM reanalysis. The colors indicate the speed and are capped at 0.25 m/s. The vectors are normalized by their corresponding speed and thus only represent the direction of the currents. The three black solid lines indicate the 50, 100, and 200 m isobaths, respectively.

constitutes an extension of the traditional EOF to deal not only with the spatial but also the temporal correlations to identify the spatial patterns of the propagating features (Weare and Nasstrom, 1982; Chen and Harr, 1993). EEOF is an EOF analysis with a modified data matrix. In EOF, each row vector represents a data map (P locations) at one time instance and each column vector represents a time series (M time instances) at a specific location of the data map. The EOF data matrix N, in this case, has dimensions of M by P as shown below

$$N = \begin{pmatrix} n_{1,1} & n_{1,2} & \cdots & n_{1,P} \\ n_{2,1} & n_{2,2} & \cdots & n_{2,P} \\ \vdots & \vdots & \vdots & \vdots \\ n_{M,1} & n_{M,2} & \cdots & n_{M,P} \end{pmatrix}. \quad (2)$$

An EOF analysis uses the variance matrix to define the periodic signals. Each row vector of an EEOF data matrix, on the other hand, contains not only the data map at a given time but also at some series of times into the past or future. In this study, we perform a 36-hour time lag EEOF analysis to the hourly data sets with 6-hour increment. The row vector is extended as

$$n_t = \left(n_{t,1} \cdots n_{t,P} n_{t+6,1} \cdots n_{t+6,P} n_{t+12,1} \cdots n_{t+12,P} \cdots n_{t+36,1} \cdots n_{t+36,P}\right), \quad (3)$$

where t varies from 1 to M-36. The data matrix has dimensions of M-36 by 7*P. Thus, an EEOF analysis on the matrix applies lagged auto-covariance matrix to find both the propagating and/or periodic signals.

An EOF analysis of the SCS SSH has been performed previously at the seasonal and interannual time scales using altimetry data (Shaw et al., 1999; Ho et al., 2000; Chu et al., 2003; Fang et al., 2006). In our case, we focus on the SSH variations on the time scale of days as there is no persistent SCSWC in winter. To do so, we remove the monthly mean and conduct a 3-month EEOF analysis for every winter season starting from December 1 for the 22-year period (1994 to 2015). The results discussed below are for December 1994 to February 1995 only. We choose this specific winter season because there exists one of the longest SCSWC occurrences during the 22-year analysis, from 7 to 13 December 1994. More importantly, there exists a 3-day period with quasi-constant wind stress and SSH within this event as shown below. This provides a wonderful opportunity to reveal the dynamics of the SCSWC in both the cross-shore and alongshore direction.

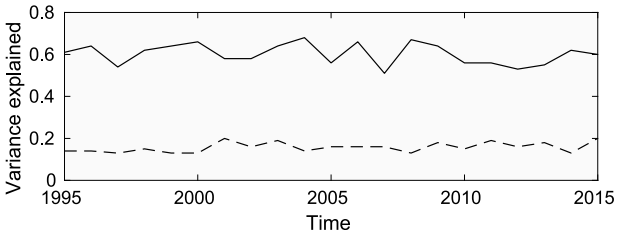

Fig. 5. Total SSH variance explained by the leading mode, Ekman transport mode (solid line), and the second mode, topographic mode (dashed line) in each winter (DJF) season.

However, sometimes EEOF results are hard to interpret and can be misleading if the time lag is not chosen with care (Monahan et al., 1999; Hannachi et al., 2007) when there are strong standing waves or a dipole in the primary EOF pattern. In this study, the most significant mode is a standing wave mode. We chose a 36 h lag to avoid this, which is much less than the first zero autocorrelation function (Monahan et al., 1999) of the leading EOF mode time series for both SSH and wind stress, 127 h. Time lags from −36 to 0 h with 6 h increment are used in the EEOF analysis. Time lags shorter and longer (still shorter than 127 h) than 36 h are also tested and the results are not sensitive to our choice of time lag.

SSH EEOF analyses over the entire 22-year period all show two dominant modes, the Ekman transport mode (leading mode) and the coastal topographic wave mode (second mode). During the 22-year reanalysis period, these two modes explain an average of 77% of the total SSH variance. The first and second SSH EEOF modes account for 61% and 16% of the total variance, respectively (Fig. 5). There are 6 winters when the third SSH EEOF explains more than 10% of the total variance and all of these are either from an eddy mode due to the existence of one or two eddies in the deep basin or the Kuroshio intrusion mode. For instance, the third SSH EEOF mode from December 1994 to February 1995 is a Kuroshio intrusion mode due to the intrusion of Kuroshio through Luzon Strait (Fig. 2a), and it explains 10% of the total variance. Since these low energy modes are not consistent, have very small SSH anomaly over the continental shelf and thus a very small contribution to the SCSWC, we choose to only analyze the first two dominant modes.

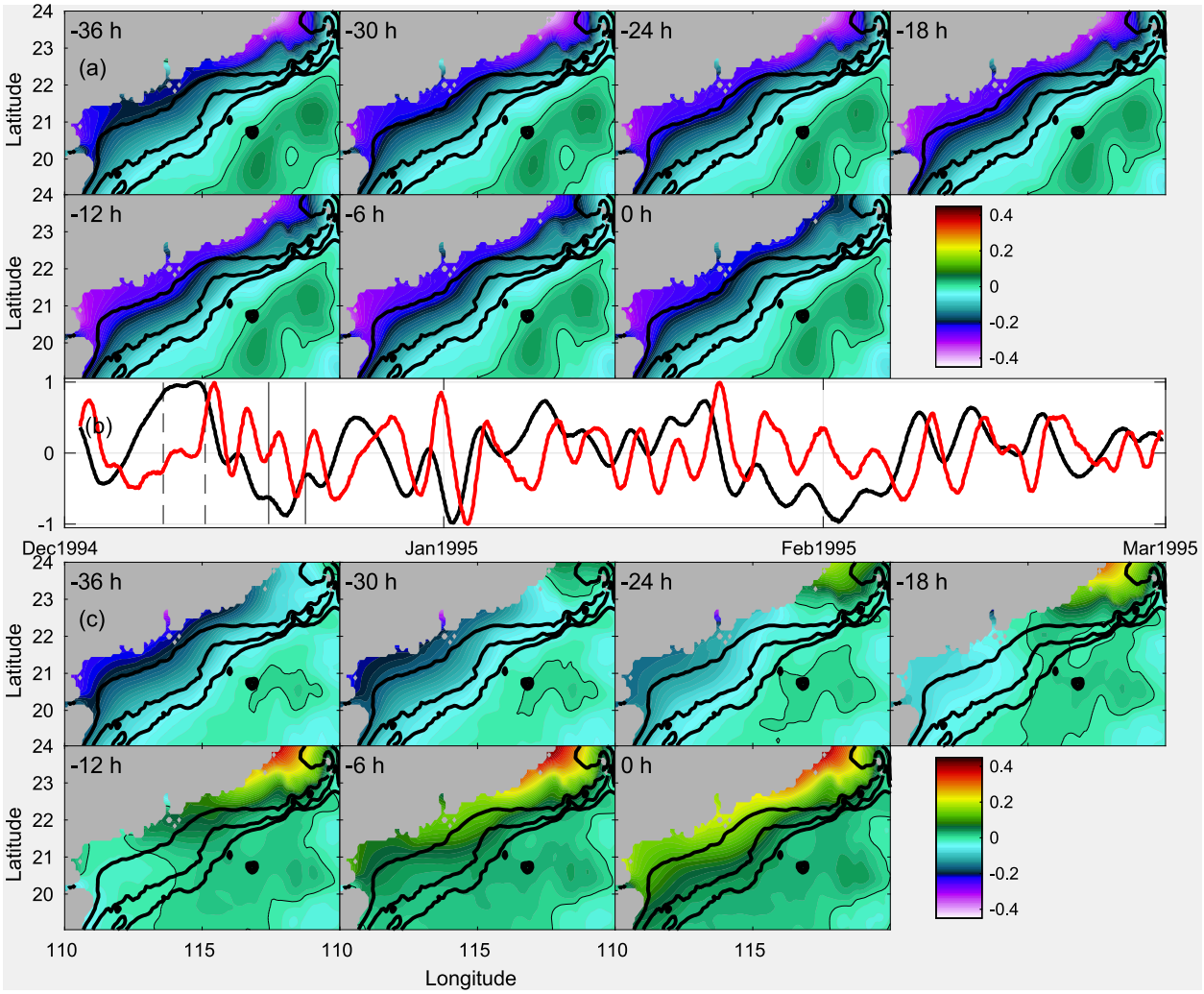

Fig. 6. The spatial pattern of the first EEOF mode (a, meters), the normalized expansion coefficient time series (b), and the spatial pattern of the second EEOF mode (c, meters) of SSH from December 1994 to February 1995 from the HYCOM reanalysis. In (b), the time series are normalized by their corresponding magnitude so that these values range from −1 to 1, with the black curve representing the first mode and red indicating the second mode. Tick marks denote the beginnings of the designated months. The vertical black dashed lines indicate the period when the expansion coefficients of the first mode are almost a constant value 1. The vertical solid black lines represent the period for the strong wind case. The EEOFs (a, and c) are inflated by the factor of the corresponding magnitude of their expansion coefficient time series. The three thick black solid lines in (a) and (c) indicate the 50, 100, and 200 m isobaths, respectively. The thin black lines in (a) and (c) indicate the 0 m contour. The time lag is shown in the upper left corner of each panel.

5.1. EEOF of SSH

The first SSH EEOF mode indicates a standing wave explaining 61% of the total SSH variance (Fig. 6a). It shows a negative SSH anomaly over the continental shelf region that increases offshore. The near zero magnitude of SSH anomaly along the shelf break indicates that the standing wave has its node along the shelf break and antinode along the coast line. This suggests that this mode causes the SSH to move up and down over the continental shelf while the SSH along the shelf break remains essentially the same. The magnitude of the SSH anomaly varies slightly during the 36-hour period but its pattern remains the same. Please note that the mode expansion coefficient time series (Fig. 6b) is normalized by its magnitude so that its range is from −1 to 1 and the mode is amplified accordingly. This first mode (Fig. 6a) indicates an amplitude of .4 m, comparable to the range of mean SSH over the study domain, which is .45 m (Fig. 2b). The expansion coefficient time series (Fig. 6b, black) shows a 7-day period from 7 GMT on 6 December to 17 GMT on 13 December 1994 with consecutive positive values. There exists a more than 3-day period from 3 GMT on 9 December to 13 GMT on 12 December 1994 (Fig. 6b, dashed vertical black lines) with an almost constant value of 1. To reconstruct the SSH anomaly associated with a mode at any particular time t, the SSH anomaly is obtained by weighted average of the mode at time lag δ multiplied by the expansion coefficient at time $t-\delta$ over the 36-hour period (Hannachi et al., 2007). In this case, δ varies from −18 to +18 with 6 h increment. The SSH anomaly at 15 GMT on 11 December 1994 is reconstructed and composited with the monthly mean (Fig. 7a) to show that this mode is able to reverse the cross-shore pressure gradient and thus the surface geostrophic flow over most of the shelf, but not the shallower region (< 50 m) to the west of 115° E where SSH still indicates a weak offshore pressure gradient force. The SCSWC can be clearly seen from the near-surface currents at the same time instant (red arrows, Fig. 7a), from northeast of Hainan Island to Taiwan Strait. The strongest currents are more than .3 m/s. But there are still weak southwestward currents to the west of 115°E over the shallowest water along the coast.

The second EEOF mode suggests a typical coastal topographic wave development/propagation over a 36-hour period, which explains 14% of the total SSH variations (Fig. 6c). It demonstrates a negative SSH anomaly that propagates southwards over the shelf from −36 to −24-hour lag, a positive SSH anomaly develops at −24-hour lag near Taiwan Strait and propagates southwards and reaches Hainan Island at 0-hour lag. The phase speed of the topographic wave estimated from the SSH

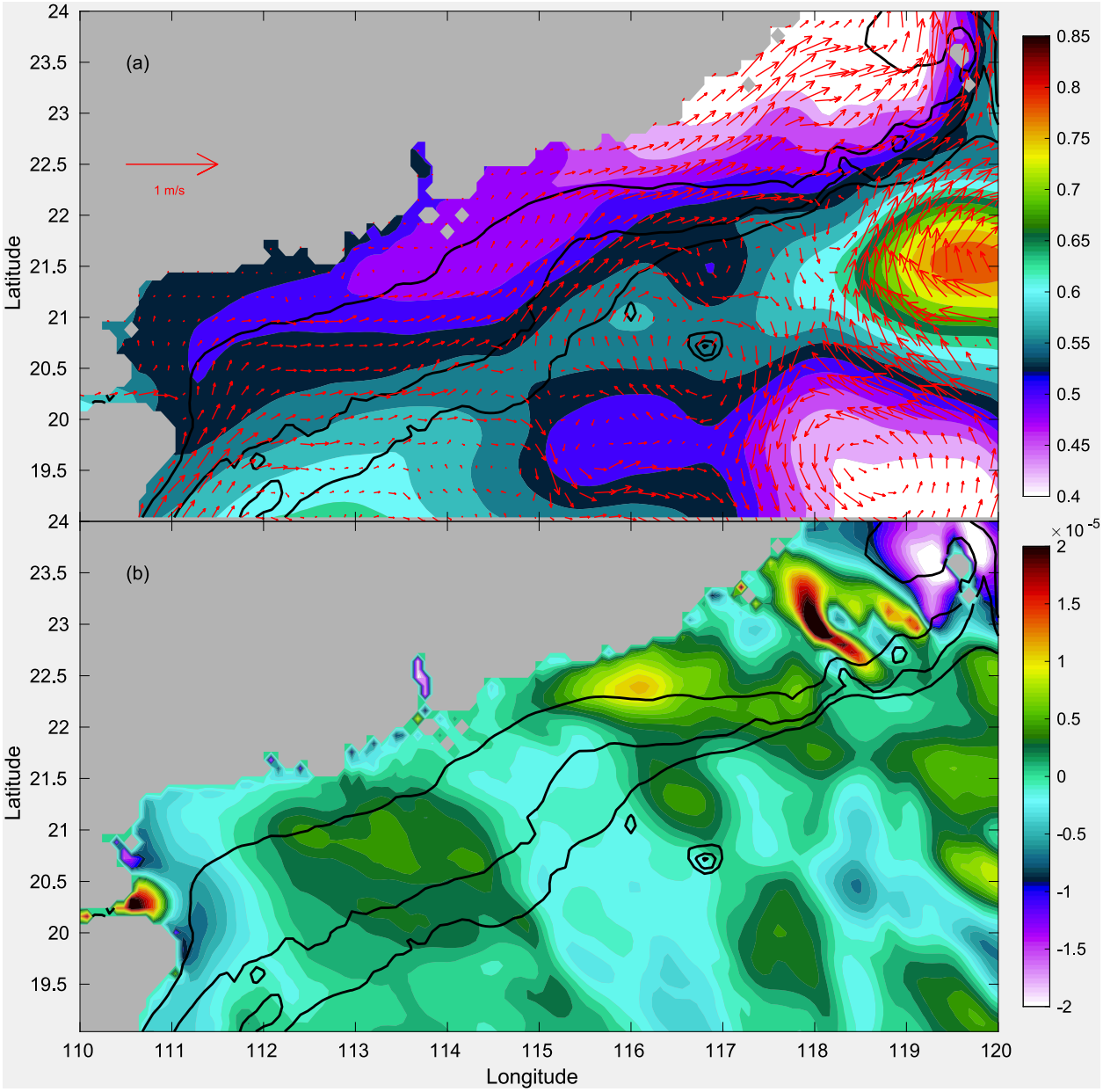

Fig. 7. The composite of the monthly mean SSH (meters) and the SSH anomaly reconstructed from the first EEOF mode overlaid with the near-surface currents (m/s, red) averaged over the top 50 m (a), and the alongshore pressure gradient force (m/s^2) associated with the SSH anomaly reconstructed from the first EEOF mode (b) at 15 GMT on 11 December 1994. The three black solid lines indicate the 50, 100, and 200 m isobaths, respectively.

anomaly along the coast of China (Fig. 8a) is 12.8 m/s, which agrees well with the coastal topographic waves estimated by Jacobs et al. (1998).

5.2. EEOF of wind stresses

The first EEOF mode of the wind stresses also shows a standing pattern explaining 64% of total wind stress variabilities (Fig. 9a). The spatial pattern indicates a southwestward oriented band of strong positive wind stress anomaly emanating from Taiwan Strait. The strong wind stress anomaly gradually decreases to the southeast and northwest of the band. The magnitude of the mode changes with time. For example, the strong positive wind stress anomaly extends southwestwards from Taiwan Strait with time from −36-hour lag to −18-hour lag but its pattern remains with time. The mode expansion coefficient time series (Fig. 9b, black) suggests a 1-week period, the same as SSH (Fig. 6b, black), of consecutive positive wind stress anomaly (i.e. wind relaxation) from 0 GMT on 6 December to 8 GMT on 13 December 1994. The time period with the consecutive coefficient bigger than 0.85 is marked between the two vertical black dashed lines from 3 GMT on 9 December to 3 GMT on 12 December 1994.

The second mode of the wind stresses suggests a reversal process of the wind stress (Fig. 9c) anomaly over the shelf. The positive wind stress anomaly decreases from −36-hour lag to −24-hour lag and moves southwestwards at the same time. The negative wind stress anomaly occurs at −24-hour lag at Taiwan Strait, grows stronger and extends southwestwards from −24-hour lag to 0-hour lag. The second EEOF wind stress mode accounts for 15% of the total variance.

5.3. Dynamics of SSH variation

The expansion coefficient time series of the first SSH EEOF mode (Fig. 6b, black) is highly correlated with the time series of the first wind stresses EEOF mode (Fig. 9b, black), significant to the 99% confidence

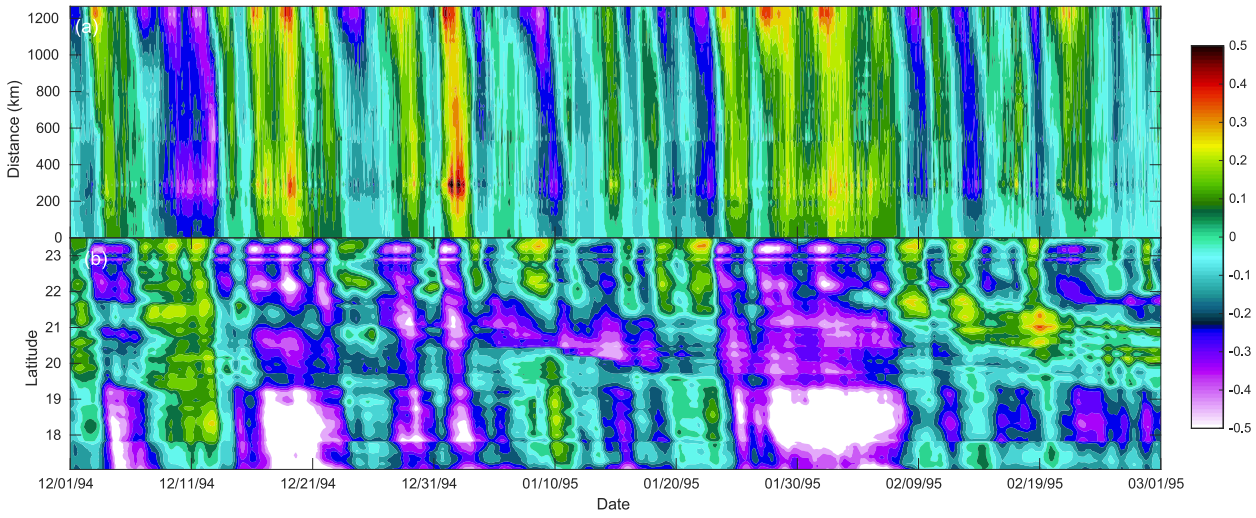

Fig. 8. Hovmöller plot of SSH anomaly (a, meters) along the Chinese coast (black dots in Fig. 1a), and the upper 50 m-average alongshore current (b, m/s) along a path defined by the black line in Fig. 1a from the HYCOM reanalysis for the dates 1 December 1994 to 28 February 1995. Tick marks denote the beginnings of the designated days. The y-axis in (a) defines points along the coast with zero starting near Hainan Island and the maximum value ending near Taiwan Strait. The events at the northern areas propagate to the south indicated by a slight tilt in the vertical streaks from the upper left to the lower right.

level, with correlation coefficient of 0.95. The time lag associated with this correlation is 10-hours and with the variation of wind stress leading the SSH variation. The positive wind stress anomaly implies alongshore wind relaxation. And thus, this high correlation suggests that wind relaxation leads to a negative SSH anomaly over the shelf and wind bursts lead to positive SSH anomalies. This is the SSH setdown/setup due to the Ekman transport, defined below.

$$U_e = \frac{\tau_v}{\rho_o f}, \tag{4}$$

where τ_v is the alongshore wind stress, ρ_o is a reference density for seawater, and f is the Coriolis parameter. The negative alongshore wind stress anomaly (wind burst) pushes water to the right side of its direction to generate a positive SSH anomaly over the continental shelf. And during wind relaxation, the positive alongshore wind stress anomaly, pushes water to the right of the wind stress anomaly direction to generate offshore Ekman transport. Total Ekman transport along the 200 m isobath with strongest wind stress anomaly on 11 December 1994 is calculated as 22 Sv (offshore). At this rate, it takes only 21 min to move enough water (2.8×10^{10} m^3, the area times the SSH anomaly due to the Ekman mode) out of the continental shelf to generate the negative SSH anomaly on that day. The excess water is compensated by the inshore currents along the sea floor to support the costal upwelling. As shown in Fig. 7a, the wind relaxation itself is able to generate the SSH anomaly to reverse the mean SSH gradient over the whole shelf to create northeastward currents via geostrophic balance.

The expansion coefficient time series of the second SSH EEOF mode (Fig. 6b, red) is also highly correlated with the time series of the second wind stress EEOF mode (Fig. 9b, red) significant to the 99% confidence level. The correlation coefficient is 0.92 associated with a time lag of 12 h, which suggests that the wind stress anomaly reversal leads the generation/propagation of the topographic waves by 12 h. The wind stress anomaly reversal (Fig. 9c) indicates that the generation/propagation of the coastal topographic waves is the result of the strong, sudden wind events, which agrees with Jacobs et al. (1998). The wind burst (negative wind stress anomaly) enhances the propagation of coastal topographic waves with positive SSH anomalies that can reverse transport through Taiwan Strait (Ko et al., 2003). The wind relaxation, the positive stress anomaly, is associated with the propagation of topographic waves with negative SSH anomalies.

6. Alongshore dynamics

In this section, we assume a slab model and compare the two alongshore forces, pressure gradient force and wind stress. The idea of treating the SCS continental shelf in winter as a slab is not new. Almost all of the previous research on this topic treat the SCSWC in winter as a barotropic process since strong wind and surface cooling in winter work together to make the water well mixed over the shelf. Thus, we treat the alongshore dynamics as governed (Chiang et al., 2008) by

$$\frac{\partial v}{\partial t} + fu = -g\frac{\partial SSH}{\partial y} + \frac{\tau_v}{\rho_o H} + Fri, \tag{5}$$

where, u and v are depth-averaged cross-shore and alongshore velocities, respectively, g is the gravitational parameter, H is the water depth, and Fri is the friction that is always against the alongshore flow. The first right hand term is the pressure gradient force and the second represents the depth-average of the alongshore kinematic wind stress. If there exists a long enough period that we can assume a steady state, Eq. (5) is the same as the alongshore equation of the arrested topographic wave (Csanady, 1978).

6.1. Wind-relaxation

The 3-day period from 3 GMT on 9 December to 3 GMT on 12 December 1994 is taken to represent the wind relaxation case. Both wind stresses and SSH are almost constant with time (vertical black dashed lines on Figs. 6b, 9b) and thus we treat it as a steady state. The first SSH EEOF mode clearly demonstrates that wind relaxation can reverse the cross-shore pressure gradient force from offshore (Fig. 2b) to onshore (Fig. 7a). It also indicates that wind relaxation increases the alongshore pressure gradient force from northeast of Hainan Island to Taiwan Strait over the shelf. Fig. 7b illustrates that the alongshore pressure gradient force at 15 GMT on 11 December 1994 associated with the first SSH EEOF mode is mainly positive along the shelf. Thus, this is the period with weaker wind stresses and stronger alongshore pressure gradient force than the monthly mean values (Table 1). The area-average of the four terms in Eq. (5) over the continental shelf in the domain shallower than 200 m isobath is summarized in Table 1. During this period of wind relaxation, the sum of the alongshore pressure gradient force and the depth-average kinematic wind stress ($-g\frac{\partial SSH}{\partial y} + \frac{\tau_v}{\rho_o H}$) are mainly positive over the continental shelf (Fig. 10a). The area-average of the pressure gradient force is 2.2×10^{-6} m/s^2 and the depth-average kinematic wind stress over the shelf in the domain shallower

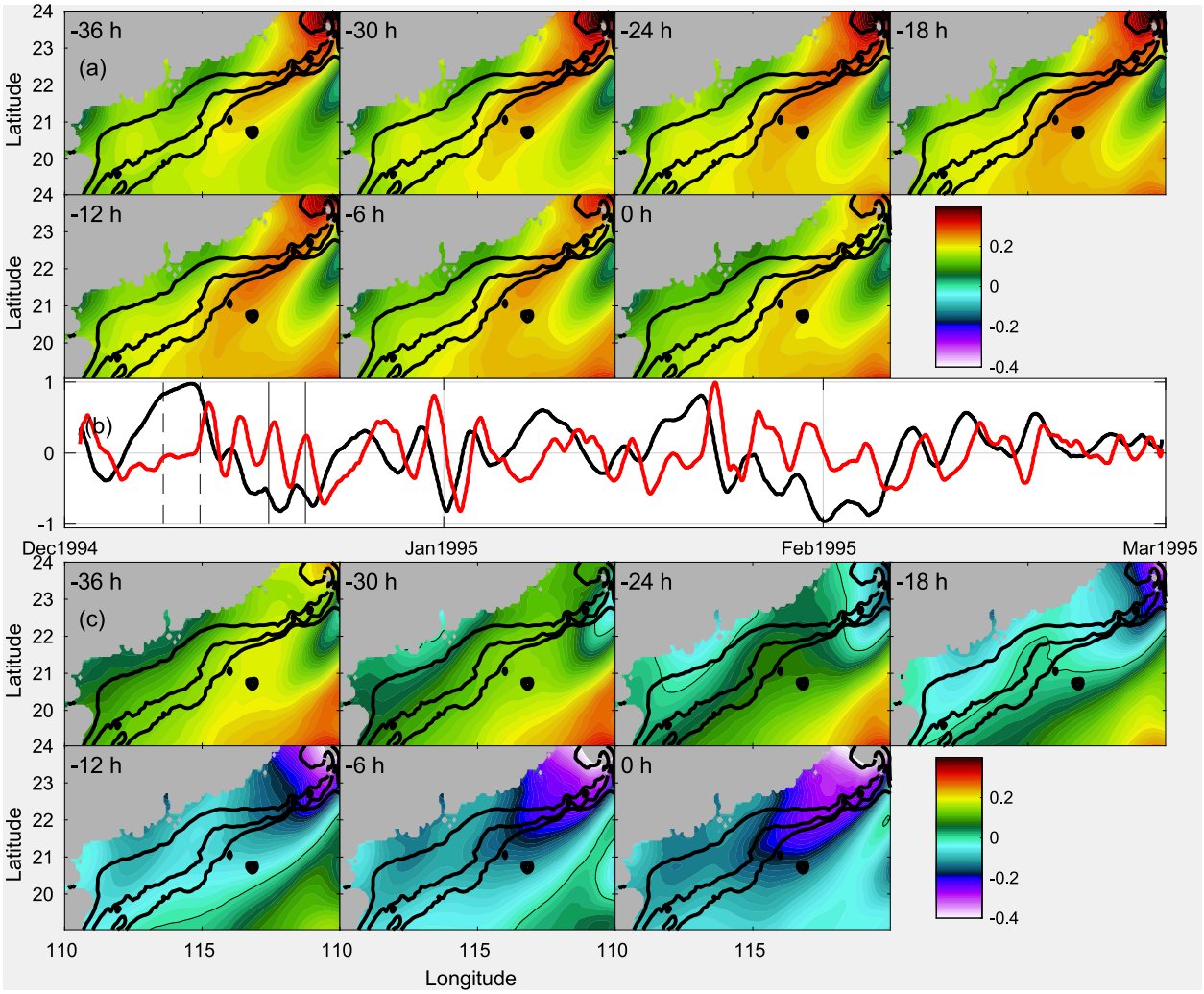

Fig. 9. The spatial pattern of the first EEOF mode (N/m^2) from the HYCOM reanalysis (a), the normalized principle component time series (b), and the spatial pattern of the second EEOF mode (N/m^2) of wind stresses (c) from December 1994 to February 1995. The time series in (b) are normalized by their corresponding magnitude so that these values range from −1 to 1 with the black curve representing the first mode and red indicating the second mode. The vertical black dashed lines indicate the period when the expansion coefficients are almost a constant value 1. The vertical solid black lines represent the period for the strong wind case. Tick marks denote the beginnings of the designated months. The EEOFs (a, and c) are inflated by the factor of the corresponding magnitude of their time series. The three thick black solid lines in (a) and (c) indicate the 50, 100, and 200 m isobaths, respectively. The thin black lines in (a) and (c) indicate the 0 N/m^2 contour. The time lag is shown in the upper left corner of each panel.

Table 1
Comparison of the four terms (10^{-6} m/s^2) in Eq. (5), area-averaged over the continental shelf in the domain shallower than 200 m isobath for three different periods in December 1994. PGF denotes alongshore pressure gradient force, wind stress is the alongshore wind stress, Coriolis denotes Coriolis force, and Friction denotes the alongshore friction force that calculated as a residual of the other three terms.

	PGF	Wind stress	Coriolis	Friction
Wind relaxation 9–12 Dec 1994	2.2	−0.73	0.97	−0.50
Wind burst 17–20 Dec 1994	0.30	−5.8	−2.4	3.1
December 1994 average	0.80	−3.7	−1.3	1.6

than 200 m is -0.73×10^{-6} m/s^2 (Table 1). This indicates that the magnitude of the alongshore pressure gradient force is larger than the wind stress. As a result, the water flows alongshore northeastward to generate a negative *Fri* (-0.50×10^{-6} m/s^2) and also offshore to generate a positive Coriolis force (0.97×10^{-6} m/s^2) to balance the force (Table 1). The most dominant force during the wind relaxation period is the alongshore pressure gradient force.

But along the coast to the west of 116°E in waters shallower than 50 m, the sum of these two forces is mainly negative (Fig. 10a) suggesting that the water flows southwestward to generate a positive *Fri*. This agrees well with the sandwich structure of the SCSWC as illustrated by Qiu et al. (1985) and Guan (1993) and is also consistent with what we see from the SSH pattern and near-surface currents (Fig. 7a). What it means dynamically is that the depth-average wind stress dominates along the coast due to the shallower water depths even though the wind stress is weaker along the coast (Figs. 2c and 8a).

Another region with negative force on the continental shelves is to the west–northwest of Dongsha Island (Fig. 10a). The alongshore pressure gradient force from the Ekman mode over this region is almost zero (Fig. 7b), which indicates that the SSH anomaly contours associated with the Ekman mode are almost parallel to the alongshore direction over the region. This suggests that the currents in this region should be further north of east. As illustrated by Fig. 7a, this is the region where the direction of the near-surface currents is 50° –60 ° north of east. Changing the alongshore direction to 50° produces the positive forces over the region.

6.2. Strong wind

The 3-day period from 17 GMT on 17 December to 17 GMT on 20 December 1994 is taken to represent the strong wind period (thin vertical black lines on Figs. 6b and 9b). During this period, the wind stresses are strong and consistently southwestward. The alongshore

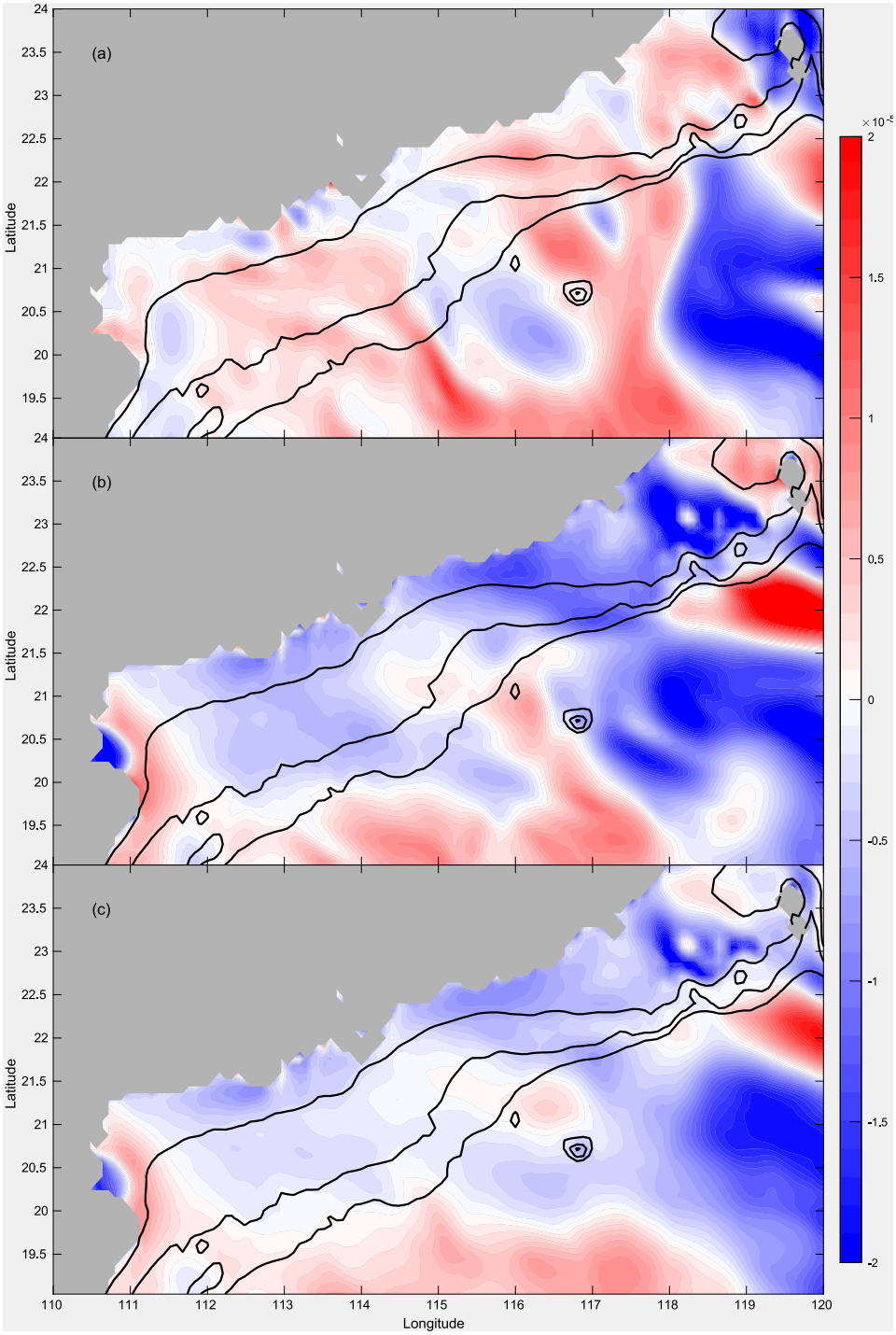

Fig. 10. The sum of the alongshore pressure gradient force and the depth-average alongshore wind stresses (m/s^2, $-g\frac{\partial SSH}{\partial y}+\frac{\tau_v}{\rho_o H}$,) during 9 to 12 December (a), 17 to 20 December (b), and December 1994 (c). The three black solid lines indicate the 50, 100, and 200 m isobaths, respectively.

pressure gradient force anomaly associated with the first EEOF mode has the same pattern as the one with wind relaxation (Fig. 7b) but in opposite direction, which is negative. Relative to the mean state, this wind burst period has stronger wind stress (-5.8 × 10^{-6} m/s^2) and weaker alongshore pressure gradient force (0.30 × 10^{-6} m/s^2), opposite to the wind relaxation case (Table 1). The sum of the alongshore pressure gradient force and the wind stress are negative over the continental shelf (Fig. 10b). This force drives the water southwestward to generate positive friction (3.1 × 10^{-6} m/s^2) and inshore to generate a negative Coriolis force (-2.4 × 10^{-6} m/s^2) to balance the force. The most dominant force during this period is the wind stress while the alongshore pressure gradient force is the least important (Table 1).

For both wind relaxation and strong wind cases, one needs to ignore the pattern at depths greater than 200 m where the assumption of a slab model (Eq. (5)) is no longer valid. In the deep basin, the pattern is fully dominated by the pressure gradient force as the depth-average kinematic wind stress is practically negligible at these depths.

In the wind relaxation case, we assume a steady state since alongshore wind stresses and SSH are almost constant. In the strong wind case, SSH and alongshore wind stresses can change as much as 50% (Figs. 6b, 9b). The time-average is taken to represent the steady state.

Most of the wind relaxation periods are shorter than 3 days and thus cannot be treated as steady state. In those cases, wind relaxation generates positive alongshore velocity tendency ($\frac{\partial v}{\partial t}$) to slow down the southwestward currents and eventually overturns and generates a counter-wind SCSWC.

7. Observed features and the origin of the SCSWC

Below, we apply the dynamics from Sections 4 and 5 to explain some of the observed features of the SCSWC and define the origin of the SCSWC.

7.1. Why there is no monthly mean SCSWC in winter

It is clear that the monthly mean SSH in December 1994 (Fig. 2b) does not support northeastward geostrophic surface currents as shown in Fig. 4. However, the mean SSH pattern supports a positive alongshore pressure gradient force. According to previous studies, this would generate SCSWC persisting in the winter season. However, our results indicate that it is the sum of the alongshore pressure gradient force and the wind stresses that determines the ageostrophic currents, not the pressure gradient force alone. In this section, we perform a similar alongshore force comparison the same as what we did in Section 6 but for the monthly mean wind stresses (-3.7×10^{-6} m/s^2) and alongshore pressure gradient force (Table 1, 0.80×10^{-6} m/s^2). The spatial pattern of the sum of these two forces (Fig. 10c) over the continental shelf are very similar to the pattern in strong wind case (Fig. 10b) except that the magnitude is smaller. This clearly demonstrates the dominance of the monthly mean wind stresses over the alongshore pressure gradient force. Monthly mean alongshore flow also follows the mean wind towards the southwest. Thus, the SCSWC cannot be persistent over the winter season.

7.2. The origin of the SCSWC

Most previous research concludes that the SCSWC originates from Hainan Island. Chiang et al. (2008) further suggested that SCSWC originates from the Gulf of Tonkin, Vietnam. Since the first SSH EEOF mode indicates an Ekman mode that covers the whole continental shelf, does this mode support the opinion that the SCSWC originates from the southern shelf near Hainan Island?

Four SSH fields 12 h apart starting from 12 GMT on 6 December 1994 are plotted to demonstrate the onset of the SCSWC (Fig. 11a). They indicate that lower SSH (.6 m contour — cyan color) is moving southwestwards along the continental shelf from the northern shelf. The composite (Fig. 11b) of the monthly mean SSH and the anomaly associated with the Ekman mode (Fig. 11c) suggests that the wave like feature we often observe in the daily-average SSH animation (Section 5) is generated by the Ekman effect and not by the topographic waves. This is really due to the fact that the mean SSH is lower to the northern shelf (Fig. 2b) and the SSH anomaly varies relatively uniformly in the cross-shore direction (Fig. 6a).

When winds start relaxing on 6 December, the Ekman effect generates negative SSH anomaly over the whole shelf. The negative SSH anomaly is weak before 0 GMT on December 7 (Figs. 11c1 and 11c2) and only able to reverse the SSH cross-shore gradient to the east of 117°E (Figs. 11b1 and 11b2) since the mean SSH gradient is smaller there between 50 and 200 m isobath (Fig. 2b). As winds continue relaxing, the negative SSH anomaly becomes stronger (Figs. 11c3 and 11c4) and is able to reverse the mean SSH gradient to the east of Hainan (Fig. 11b4) between the 50 and 200 m isobaths. The counter-wind currents first appear only at the very north of the continental shelf (red arrows, Fig. 12a), move southwards (Figs. 12b and 12c) and finally cover the whole shelf from east of Hainan to south of Taiwan Strait at 0 GMT on December 8, 1994 (Fig. 12d). Thus, these results show that the SCSWC in winter originates in the area south of Taiwan Strait when the winds relax and extends southwards over the shelf as the wind continues to relax. But is this always the case?

A Hovmöller diagram of the near surface alongshore currents averaged over the top 50 m along a SCSWC path over the shelf is shown in Fig. 8b. The path (black line, Fig. 1a) is defined as the 125 m isobath from 17°N to 21°N, and then a straight line from (115.36°E, 21.02°N) to (119.04°E, 23.5°N). The tilt in the vertical streaks from the upper left to the lower right indicating the SCSWC extends from the area south of Taiwan Strait southwestwards, agreeing with the dynamics mentioned above. The strongest SCSWC event in this season can reach to 17.5°N, more than 1000 km long. But other events, like the one on February 9, 1995, only exist in the northern shelf, to the north of 21°N. If the SCSWC originates from Gulf of Tonkin, or Hainan Island, the tilt in the vertical streaks should be from lower left to the upper right. But that is not the case.

7.3. Increasing SCSWC downstream

Our results also clearly illustrate the coexistence of the SCSWC sandwiched between the southwestward Guangdong coastal currents from 110°E to 117°E (Fig. 12) and the cyclonic upper ocean circulation over the central basin during wind relaxation periods in winter season, that is consistent with previous findings (Qiu et al., 1985; Guan, 1993). Between the 50 m and 200 m isobaths, the positive monthly mean cross-shore pressure gradient force is strongest near Hainan and becomes smaller northeastward from 111°E to 116°E (Fig. 2b). The monthly mean currents averaged over the top 50 m are stronger near Hainan and becomes weaker northeastward from 111°E to 116°E (Fig. 4).

Relative to the mean SSH gradient, the negative SSH anomaly associated with the first mode varies uniformly in the cross-shore direction (Fig. 11c) along the whole shelf. The negative cross-shore pressure gradient force associated with the Ekman mode balances the mean positive pressure gradient force and eventually reverses it when winds relax. Because the mean cross-shore pressure gradient force is strongest near Hainan, the combined (mean + Ekman mode) cross-shore pressure gradient force is negative but has a smaller magnitude than that to the northeast of Hainan along the shelf to 116°E. Due to geostrophy, the northeastward SCSWC is weaker near Hainan and increases downstream. Fig. 12d shows the strongest SCSWC occurs at 115°E and agrees well with the previous observations (Zhong, 1990).

8. Conclusions

In this study, we investigate the generation mechanism of the counter-wind characteristics of the SCSWC in the winter seasons using output from a 22-year (1994–2015) HYCOM global reanalysis. The reanalysis is forced with atmospheric forcing from the 0.3125° hourly NCEP CFSR dataset and a wind stress formulation that takes into account the ocean surface currents. Because of the latter, the wind stress is bigger over the SCSWC than those calculated only by 10-m wind velocities. We performed two analyses: 1) an EEOF analysis on the hourly SSH and alongshore wind stress in each winter and, 2) a comparison of the alongshore pressure gradient force and the alongshore wind stress.

The EEOF analysis reveals that the leading SSH EEOF mode, which explains more than 60% of the total variance, is the direct result of Ekman transport. During wind bursts, the water is pushed inshore and piles up along the coast. When winds relax, the Ekman transport is offshore. The closer to the coast, the bigger change of the SSH. The second SSH EEOF mode represents the generation/propagation of the coastal topographic waves that are excited by the wind change. When winds relax, it is associated with the propagation of the waves with negative SSH anomaly. Monthly mean SSH demonstrates a strong positive cross-shore pressure gradient force. The Ekman effect associated with wind relaxation can produce a large enough pressure gradient to reverse the

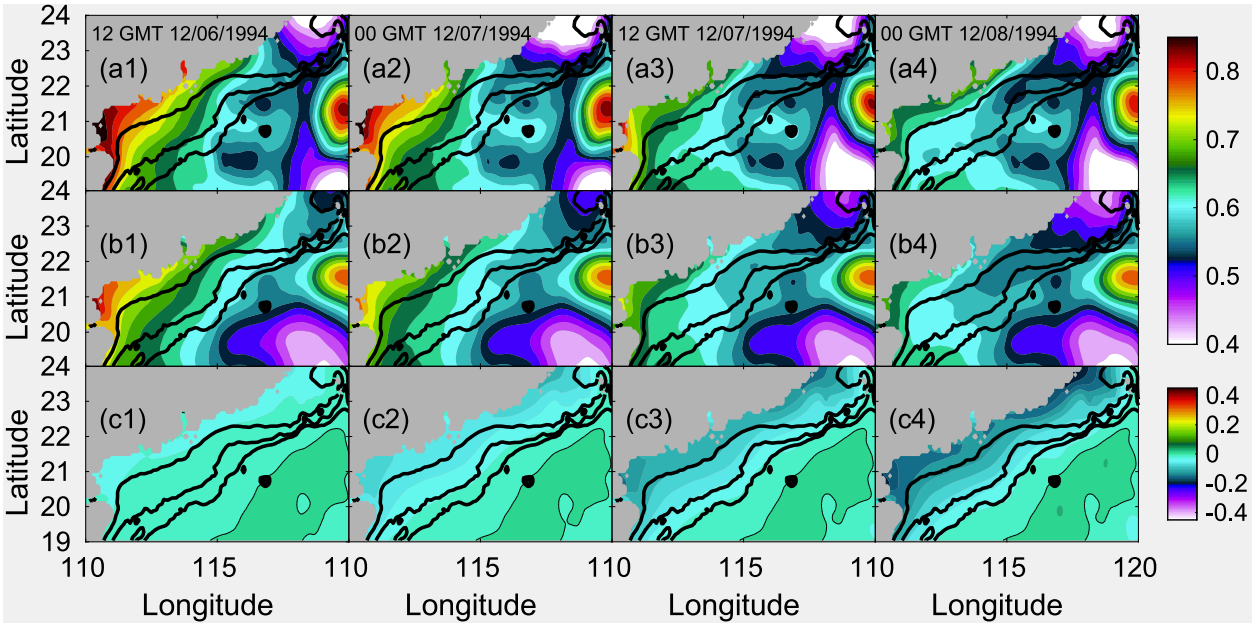

Fig. 11. SSH fields (meters) from the HYCOM reanalysis (a), composite of the mean SSH and the SSH anomaly reconstructed from the first EEOF mode (b), the SSH anomaly reconstructed from the first EEOF mode (c) starting from 12 GMT on 6 December 1994 (1) to 0 GMT on 8 December 1994 (4). The thin black lines in (c) indicate the 0 m contour. The three thick black solid lines indicate the 50, 100, and 200 m isobaths, respectively.

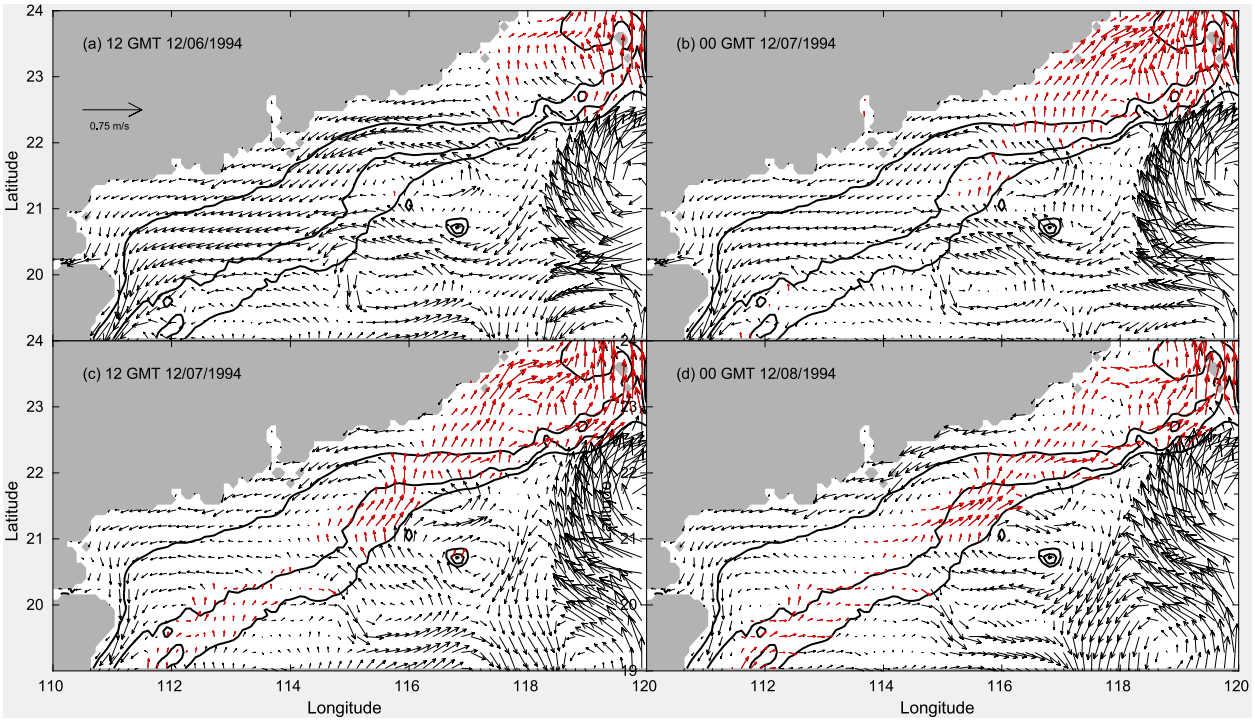

Fig. 12. Near-surface currents (m/s) averaged over the top 50 m starting from 12 GMT on 6 December 1994 (a) to 0 GMT on 8 December 1994 (d). The reference vector is shown in the upper left corner of (a). The red arrows represent the South China Sea Warm Current with positive alongshore flow. The three thick black solid lines indicate the 50, 100, and 200 m isobaths, respectively.

cross-shore pressure gradient force to generate northeastward counter-wind flow. The propagation of the topographic waves associated with wind relaxation is secondary to enhance the process. Because the mean cross-shore pressure gradient is smaller in the area south of Taiwan Strait than over the rest of the shelf, the Ekman effect reverses the cross-shore pressure gradient in the northern shelf first. Thus, the SCSWC originates from the northern shelf, in the area south of Taiwan Strait.

SSH EEOF analysis also indicates that wind relaxation increases the alongshore pressure gradient force while wind bursts decrease the alongshore pressure gradient force. During the 3-day wind relaxation period in December 1994, the stronger positive alongshore pressure gradient force overtakes the weaker alongshore wind stresses to push the water northeastward. And in the strong wind case, the southwestward wind stresses are much stronger than the weaker than normal

northeastward alongshore pressure gradient force. Thus, the surface water follows the wind.

Declaration of competing interest

The authors declare that they have no known competing financial interests or personal relationships that could have appeared to influence the work reported in this paper.

Acknowledgments

The authors thank the editor and the anonymous reviewers for their input to improve the original manuscript. Financial support for Z. Yu and E. J. Metzger is provided by the "6.1 South China Sea Dynamics" project sponsored by the Office of Naval Research, USA under program element 0601153N. Y. Fan is funded by the "6.2 Turbulent Mixing in NCOM and HYCOM" project sponsored by the Office of Naval Research, USA under program element 062435N. Computer time was provided by the Department of Defense (DoD) High Performance Computing Modernization Program and the simulations were performed on the Cray XC40 (Conrad) at the Navy DoD Supercomputing Resources Center, Stennis Space Center, MS. The output used in the research is served at http://www.hycom.org/dataserver/gofs-3pt1/reanalysis. This is NRL contribution NRL/JA/7320-20-5015. It has been approved for public release and distribution is unlimited.

References

Bleck, R., 2002. An oceanic general circulation model framed in hybrid isopycnic-cartesian coordinates. Ocean Model. 4, 55–88.

Chao, S.Y., Shaw, P.T., Wang, J., 1995. Wind relaxation as a possible cause of the south China sea warm current. J. Oceanogr. 51 (1), 111–132.

Chassignet, E.P., Smith, L.T., Halliwell, G.R., Bleck, R., 2003. North atlantic simulations with the hybrid coordinate ocean model (HYCOM): Impact of the vertical coordinate choice, reference pressure, and thermobaricity. J. Phys. Oceanogr. 33, 2504–2526.

Chen, J.-M., Harr, P.A., 1993. Interpretation of extended empirical orthogonal function (EEOF) analysis. Mon. Wea. Rev. 121, 2631–2636.

Chiang, T.-L., Wu, C.-R., Chao, S.-Y., 2008. Physical and geographical origins of the south China sea warm current. J. Geophys. Res. 113 (C08028), http://dx.doi.org/10.1029/2008JC004794.

Chu, P.C., Wang, J., Qi, Y., 2003. Determination of the South China sea surface height variability using TOPEX/POSEIDON data. In: Proceedings of SPIE Conference on Remote Sensing of the Ocean and Sea Ice, Barcelona, Spain.

Chuang, W.-S., 1985. Dynamics of subtidal flow in the Taiwan strait. J. Ocean- Ogr. Soc. Jpn. 41, 65–72.

Chuang, W.-S., 1986. A note on the driving mechanisms of current in the Taiwan strait. J. Oceanogr. Soc. Jpn. 42, 355–361.

Csanady, G.T., 1978. The arrested topographic wave. J. Phys. Oceanogr. 8, 47–62.

Cummings, J.A., 2005. Operational multivariate ocean data assimilation. Q. J. R. Meteorol. Soc. 131, 3583–3604.

Cummings, J.A., Smedstad, O.M., 2013. Variational data assimilation for the global ocean. In: Park, S.K., Xu, L. (Eds.), Data Assimilation for Atmospheric, Oceanic, and Hydrologic Applications (Vol. II). Springer-Verlag, Berlin Heidelberg, http://dx.doi.org/10.1007/978-3-642-35088-7_13.

Fang, G., Chen, H., Wei, Z., Wang, Y., Wang, X., Li, C., 2006. Trends and interannual variability of the south China sea surface winds, surface height, and surface temperature in the recent decade. J. Geophys. Res. 111, C11S16. http://dx.doi.org/10.1029/2005JC003276.

Fang, W., Guo, P., Liu, C., Fang, G., Li, S., 2015. Observed sub-inertial current variability and volume transport over the continental shelf in the northern south China sea. Estuar. Coast. Shelf Sci. 157, 19–31. http://dx.doi.org/10.1016/j.ecss.2015.02.001.

Guan, B.X., 1986. Evidence for a counter-wind current in winter off the southeast coast of China. Chin. J. Oceanol. Limnol. 4 (4), 319–332.

Guan, B.X., 1993. Winter counter-wind current off the southeastern China coast and a preliminary investigation of its source. In: Proceedings of the Symposium on the Physical and Chemical Oceanography of the China Seas. China Ocean Press, Beijing, pp. 1–9.

Guan, B.X., Chen, S.J., 1964. The Current Systems in the Near-Sea Area of China Seas. p. 85, (in Chinese).

Guan, B., Fang, G., 2006. Winter counter-wind currents off the southeastern China coast: A review. J. Oceanogr. 62, 1–24. http://dx.doi.org/10.1007/s10872-006-0028-8.

Hannachi, A., Jolliffe, I.T., Stephenson, D.B., 2007. Empirical orthogonal functions and related techniques in atmospheric science: A review. Int. J. Climatol. 27, 1119–1152.

Helber, R.W., Townsend, T.L, Barron, C.N., Dastugue, J.M., Carnes, M.R., 2013. Validation Test Report for the Improved Synthetic Ocean Profile (ISOP) System: Part I. Synthetic Profile Methods and Algorithm. NRL memorandum report NRL/MR/7320–13-9364, http://www7320.nrlssc.navy.mil/pubs/2013/helber1-2013.pdf.

Ho, C.-R., Zheng, Q., Soong, Y.S., Kuo, N.-J., Hu, J.-H., 2000. Seasonalvariability of sea surface height in the south China sea observed with TOPEX/POSEIDON altimeter data. J. Geophys. Res. 105 13, 981-913, 990.

Hsueh, Y., Zhong, L., 2004. A pressure-driven South China sea warm current. J. Geophys. Res. 109, C09014. http://dx.doi.org/10.1029/2004JC002374.

Hu, J.Y., Kawamura, H., Hong, H., Qi, Y.Q., 2000. A review on the currents in the south China sea: Seasonal circulation, south China sea warm current and kuroshio intrusion. J. Oceanogr. 56, 607–624.

Jacobs, G.A., Preller, R.H., Riedlinger, S.K., Teague, W.J., 1998. Coastal wave generation in the bohai bay and propagation along the Chinese coast. Geophys. Res. Lett. 25 (6).

Ko, D.S., Preller, R.H., Jacobs, G.A., Tang, T.Y., Lin, S.F., 2003. Transport reversals at Taiwan strait during october and 1999. J. Geophys. Res. 108, 3370. http://dx.doi.org/10.1029/2003JC001836.

Li, R.F., Zeng, Q.C., Gan, Z.J., Wang, W.Z., 1993. Numerical simulation of the south China sea warm current and the Taiwan strait flow in winter. Progr. Nat. Sci. 3 (2), 123–129.

Li, R.F., Zeng, Q.C., Ji, Z.Z., Gun, D., 1992. Numerical simulation for a northeastward flowing current from area off the eastern Hainan island to Tsugaru/Soya strait. La Mer 30, 229–238.

Metzger, E.J., Smedstad, O.M., Thoppil, P.G., Hurlburt, H.E., Cummings, J.A., Wallcraft, A.J., Zamudio, L., Franklin, D.S., Posey, P.G., Phelps, M.W., Hogan, P.J., Bub, F.L., Dehaan, C.J., 2014. US navy operational global ocean and arctic ice prediction systems. Oceanogr. 27, 32–43.

Monahan, A.H., Tangang, F.T., Hsieh, W.W., 1999. A potential problem with extended EOF analysis of standing wave fields. Atmosphere- Ocean 3, 241–254.

Qiu, D.Z., Huang, Y.T., Chen, L.M., Guo, Z.X., 1985. Circulation structures in the studied waters. In: Comprehensive Investigations and Studies of the South China Sea, 2, ed. South China Sea Institute of Oceanology, Chinese Academy of Sciences, Science Press, Beijing, pp. 204–230, (in Chinese).

Saha, S., Coauthors, 2010. The NCEP climate forecast system reanalysis. Bull. Am. Meteorol. Soc. 91, 1015–1057. http://dx.doi.org/10.1175/2010BAMS3001.1.

Sarkisyan, A.S., Ivanov, V.F., 1971. Joint effect of baroclinicity and bottom relief as an important factor in the dynamics of sea currents. Izv. Academy of Science, USSR, Atmos. Ocean. Phy. 7 (2), 173–188, (English translation).

Shaw, P.T., Chao, S.Y., 1994. Surface circulation in the south China sea. Deep-Sea Res. I 40 (11/12), 1663–1683.

Shaw, P.T., Chao, S.Y., Fu, L.L., 1999. Sea surface height variations in the south China sea from satellite altimetry. Oceanol. Acta 22 (1), 1–17.

Shu, Y., Wang, Q., Zu, T., 2018. Progress on shelf and slope circulation in the northern south China sea. Sci. China Earth Sci. 61, 560–571. http://dx.doi.org/10.1007/s11430-017-9152-y.

Shu, Y., Xue, H., Wang, D., Xie, Q., Chen, J., Li, J., Chen, R., He, Y., Li, D., 2016. Observed evidence of the anomalous south China sea western boundary current during the summers of 2010 and 2011. J. Geophys. Res. Oceans 121, 1145–1159. http://dx.doi.org/10.1002/2015JC011434.

Su, J.L., Wang, W., 1987. On the sources of the Taiwan warm current from the south China sea. Chin. J. Oceanol. Limnol. 5 (4), 299–308.

Tian, J., Yang, Q., Liang, X., Xie, L., Hu, D., Wang, F., Qu, T., 2006. Observation of Luzon Strait transport. Geophys. Res. Lett. 33 (L19607), http://dx.doi.org/10.1029/2006GL026272.

Wang, D., Hong, B., Gan, J., Xu, H., 2010. Numerical investigation on propulsion of the counter-wind current in the northern south China sea in winter. Deep Sea Res. I 57, 1206–1221. http://dx.doi.org/10.1016/j.dsr.2010.06.007.

Wang, Q., Zeng, L., Chen, J., He, Y., Zhou, W., Wang, D., 2020a. The linkage of kuroshio intrusion and mesoscale eddy variability in the northern south China sea: subsurface speed maximum. Geophys. Res. Lett. 46, http://dx.doi.org/10.1029/2020GL087034, e2020GL087034.

Wang, Q., Zhou, W., Zeng, L., Chen, J., He, Y., Wang, D., 2020b. Intraseasonal variability of cross-slope flow in the northern south China sea. J. Phys. Oceanogr. 50, http://dx.doi.org/10.1175/JPO-D-19-0293.1.

Weare, B.C., Nasstrom, J.S., 1982. Examples of extended empirical orthogonal function analysis. Mon. Wea. Rev. 110, 481–485.

Wyrtki, K., 1961. Physical oceanography of the southeast Asian water. In: NAGA Report 2, Scientific Result of Marine Investigation of the South China Sea and Gulf of Thailand 1959–1961. Scripps Institution of Oceanography, La Jolla, California, p. 195.

Xue, H., Chai, F., Pettigrew, N., Xu, D., Shi, M., Xu, J., 2004. Kuroshio intrusion and the circulation in the south China sea. J. Geophys. Res. 109, C02017. http://dx.doi.org/10.1029/2002JC001724.

Yang, K.-C., 2006. The Non-Persistent South China Sea Warm Current (M. S. dissertation). National Taiwan Univ. Taipei, p. 48.

Yang, J., Wu, D., Lin, X., 2008. On the dynamics of the south China sea warm current. J. Geophys. Res. 113, C08003. http://dx.doi.org/10.1029/2007JC004427.

Ye, L., 1994. On the mechanism of south China sea warm current and kuroshio branch in winter - preliminary result of 3-D baroclinic experiments. Terr. Atmos. Oceanic Sci. 5 (4), 597–610.

Yu, Z., Fan, Y., Metzger, E.J., Smedstad, O.M., 2018. The wind work input into the global ocean revealed by a 17-year global hybrid coordinate ocean model reanalysis. Ocean Model. http://dx.doi.org/10.1016/j.ocemod.2018.07.009.

Yu, Z., Metzger, E.J., Fan, Y., 2017. The impact of ocean surface currents on sverdrup transport in the midlatitude north Pacific via the wind stress formulation. J. Phys. Oceanogr. 47, http://dx.doi.org/10.1175/JPO-D-16-0155.1.

Yu, Z., Metzger, E.J., Thoppil, P., Hurlburt, H.E., Zamudio, L., Smedstad, O.M., Na, H., Nakamura, H., Park, J.-H., 2015. Seasonal cycle of volume transport through Kerama gap revealed by a 20-year global hybrid coordinate ocean model reanalysis. Ocean Model. 96, 203–213. http://dx.doi.org/10.1016/j.ocemod.2015.10.012.

Zeng, Q., Li, R., Ji, Z., Gan, Z., Ke, P., 1989. Calculations of the monthly mean circulation in the south China sea (in Chinese). Sci. Atmos. Sin. 13, 127–168.

Zhong, H.L., 1990. Structures of the density circulation (in Chinese). In: Ma, Y.L., et al. (Eds.), Report of Decadal Hydrographic Series Survey of the Shelf and Adjacent Waters of the Northern South China Sea. China Ocean Press, Beijing, pp. 215–241.